Absence of strong localization at low conductivity in the topological surface state of low-disorder Sb_{2}Te_{3}

Ilan T. Rosen, Indra Yudhistira, Girish Sharma, Maryam Salehi, M. A. Kastner, Seongshik Oh, Shaffique Adam, and David Goldhaber-Gordon

Phys. Rev. B **99**, 201101 — Published 2 May 2019

DOI: 10.1103/PhysRevB.99.201101

Absence of strong localization at low conductivity in the topological surface state of low disorder Sb_2Te_3

Ilan T. Rosen,[1,2] Indra Yudhistira,[3,4] Girish Sharma,[3,4] Maryam Salehi,[5] M. A. Kastner,[6,2,7,8] Seongshik Oh,[9] Shaffique Adam,[3,4,10] and David Goldhaber-Gordon[6,2,*]

[1]*Department of Applied Physics, Stanford University, Stanford, California 94305, USA*
[2]*Stanford Institute for Materials and Energy Sciences, SLAC National Accelerator Laboratory, Menlo Park, California 94025, USA*
[3]*Department of Physics, National University of Singapore, Singapore 117551, Singapore*
[4]*Centre for Advanced 2D Materials and Graphene Research Centre, National University of Singapore, Singapore 117546, Singapore*
[5]*Department of Materials Science and Engineering, Rutgers, the State University of New Jersey, Piscataway, New Jersey 08854, USA*
[6]*Department of Physics, Stanford University, Stanford, California 94305, USA*
[7]*Department of Physics, MIT, Cambridge, Massachusetts 02139, USA*
[8]*Science Philanthropy Alliance, 480 S. California Ave, Palo Alto, California 94306, USA*
[9]*Department of Physics and Astronomy, Rutgers, the State University of New Jersey, Piscataway, New Jersey 08854, USA*
[10]*Yale-NUS College, Singapore 138614, Singapore*

We present low-temperature transport measurements of a gate-tunable thin film topological insulator system that features high mobility and low carrier density. Upon gate tuning to a regime around the charge neutrality point, we infer an absence of strong localization even at conductivities well below e^2/h, where two dimensional electron systems should conventionally scale to an insulating state. Oddly, in this regime the localization coherence peak lacks conventional temperature broadening, though its tails do change dramatically with temperature. Using a model with electron-impurity scattering, we extract values for the disorder potential and the hybridization of the top and bottom surface states.

Time-reversal invariant three-dimensional topological insulators (3D TIs) are gapped materials with inverted bulk bands. At energies within the bulk bandgap, topological surface states (TSS) are guaranteed to exist [1]. Each surface state of Bi_2Se_3 family materials is a single two-dimensional (2D) Dirac cone in which the in-plane spin is correlated with the wave vector [2, 3]. Whereas topologically trivial (conventional) 2D electron systems (2DES) are strongly insulating at low carrier densities because of Anderson (strong) localization [4], TSS are expected to be impervious to localization, even under strong disorder [5]. As far as we know, no other time-reversal invariant two-dimensional system has a metallic single-particle description in the presence of disorder – even in graphene, intervalley scattering due to disorder leads to localization [6]. Intuitively, TSS should not localize because large angle scattering is prohibited without a time-reversal symmetry-breaking spin-flip: states with opposite wavevector have opposite spin.

Localization can in principle occur in 3D TI thin films. Tunneling through the thickness of a film hybridizes the top and bottom TSS, opening a surface gap 2Δ around the Dirac point [7, 8]. The massive Dirac fermions no longer enjoy absolute protection against localization. When hybridization is small, however, large angle scattering should still be suppressed; therefore, strong localization may be suppressed at low densities where conventional 2DES would be expected to localize. Benefiting from gate-tunability and suppressed bulk conduction [9], thin film 3D TIs provide an opportunity to study the effect of spin texture on localization physics in two dimensions.

Careful study of these systems, however, has been hampered by various materials issues: defects push the Fermi levels of the binary V-VI topological compounds (Bi_2Se_3, Bi_2Te_3, and Sb_2Te_3) far from the Dirac point [10], and epitaxial mismatches between the topological insulator and the substrate introduce additional disorder [11]. Disorder decidedly affects the electrical conduction of TSS: the mobilities of typical thin film V-VI topological materials reach only of order 100 cm^2/Vs. Furthermore, while electrostatic gating can tune the Fermi level to the charge neutrality point (CNP), charged impurities obscure low density transport physics in favor of transport through charge puddles [12–14]. Consequently, insulating ($\sigma_{xx} < e^2/h$) time-reversal symmetry-protected 3D TI systems have only been seen in the thinnest films, where the clean-limit hybridization gap far exceeds room temperature [15–17].

We report transport properties of a top-gated Hall bar of a novel Sb_2Te_3-based thin film. The key components of this platform are 1) an epitaxially matched trivial insulator serves as a virtual substrate for the growth of the topological insulator, reducing defects, and 2) the topological insulator is counter-doped to bring its Fermi level close to the Dirac point, even before electrostatic gating. This materials platform, introduced in more detail in Ref. [18], offers a high mobility TSS with small and

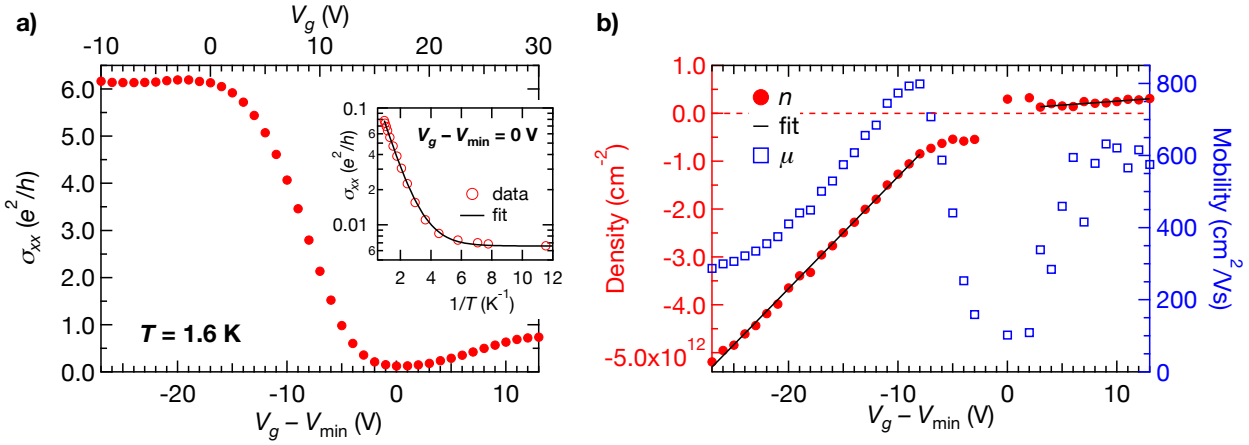

FIG. 1. Transport properties. (a) Longitudinal conductivity as a function of top gate voltage at zero field and $T = 1.6$ K. The top axis shows the actual gate voltage; the bottom axis shows the difference ΔV between the gate voltage and the conductivity minimum $V_{\rm min}$. Inset: The conductivity at $V_{\rm min}$ is described by an Arrhenius law plus a constant offset, which we attribute to Joule heating from the current bias. (b) Carrier density (left axis) extracted from the Hall slope, and the associated Hall mobility (right axis), shown versus ΔV at $T = 1.6$ K. Fits to the slope of the density (solid lines) yield $\alpha_h = 2.3 \times 10^{11}$ cm^{-2}/V on the hole side and $\alpha_e = 1.7 \times 10^{10}$ cm^{-2}/V on the electron side

comparable surface gap and disorder potential, allowing study of the electrical transport near the Dirac point. Like other Dirac metals, this film's magnetoconductance is negative and agrees with weak anti-localization (WAL) theory at high carrier densities. Strikingly, signatures of WAL persist close to the CNP, although the conductivity $\sigma_{xx} \ll e^2/h$. This feature implies the absence of scaling to strong localization, possibly associated with the topological origin of the surface states.

METHODS

Sb_2Te_3 was grown by molecular beam epitaxy. Interface engineering reduces disorder stemming from the lattice mismatch between topological insulator and substrate. A 15 quintuple layer (QL; 1 QL $\approx$ 1 nm) $(Sb_{0.65}In_{0.35})_2Te_3$ (a trivial insulator) buffer layer was grown on a sapphire substrate. Growth of the topological insulator, 8 QL Sb_2Te_3 counter-doped by 2% Ti, followed. A 2 QL $(Sb_{0.65}In_{0.35})_2Te_3$ capping layer was deposited *in situ* to protect the TI. The thickness of the capping layer was chosen as a compromise to protect the Sb_2Te_3 while not impairing the efficacy of the top gate. A 50 μm wide Hall bar was fabricated. A top gate was formed with a 40 nm alumina dielectric atop the $(Sb_{0.65}In_{0.35})_2Te_3$ capping layer. Measurements were made in a ^{3}He/^{4}He dilution refrigerator (30 mK to 1.2 K) and a ^{4}He cryostat with a variable temperature insert (1.5 K to 30 K) using standard lock-in techniques. To accurately measure the high resistances near the CNP at dilution refrigeration temperatures, some measurements were made using a high-impedance DC current source and a nanovoltmeter. All resistance (conductance) values are obtained through four-terminal measurements and are presented as two dimensional resistivity (conductivity).

Hall measurements at zero gate voltage and $T = 50$ mK yielded carrier density $n = -2.5 \times 10^{12}$ cm^{-2}, where the negative sign indicates holes rather than electrons, and mobility $\mu = 580$ cm^2/Vs. To account for variation in the Fermi level between different cooldowns, we present gate voltage as $\Delta V_g = V_g - V_{\rm min}$ where $V_{\rm min}$ is the gate voltage at which the conductivity is minimized during that cooldown (between 17 V and 20 V for all cooldowns). $V_{\rm min}$ is often associated with the CNP; however, given the presence of charge puddles in a disordered potential landscape, the CNP occurs precisely at $V_{\rm min}$ only if electrons and holes have equal mobility.

RESULTS

The zero-field resistance of the device is shown as a function of gate voltage in Fig. 1 (a). The carrier density, as extracted from fitting the Hall slope at applied fields $|B| < 0.25$ T to a single-carrier model, is shown in Fig. 1 (b) along with the Hall mobility. At gate voltages well below $V_{\rm min}$, the conductivity saturates at $\sigma_{xx} \approx 6e^2/h$, meaning the mobility $\mu \propto |n|^{-1}$. In this high-density limit, the conductivity increases logarithmically with temperature [19]. Moving toward $V_{\rm min}$, hole carriers are depleted and the conductivity drops, reaching $\sigma_{xx} < 0.01e^2/h$ at $V_{\rm min}$. As $|n|$ decreases, the temperature dependence of the conductivity evolves to an Arrhenius activation law with activation energy $\Delta_{\rm Arr} = 84$ μeV at $V_g = V_{\rm min}$ (Fig. 1 (a), inset) [19].

The resistivity in perpendicular applied fields up to

10 T at various gate voltages is shown in the supplement [19]. A sharp positive quantum coherence peak in the magnetoconductance at zero field, indicative of WAL, is observed at all gate voltages. At $\Delta V_g \leq -4$ V, the coherence peak broadens with increasing temperature (Fig. 2 (a-b)), while at $\Delta V_g \geq -4$ V, the magnetoconductance flattens or switches sign as B increases (Fig. 2 (c-d)). The lower the temperature, the lower the field at which the magnetoconductance switches sign. In a disordered system, aside from the coherence peak, there is a positive classical contribution to the magnetoresistance that changes from quadratic at low magnetic fields to linear at high magnetic fields [14, 20] and saturates in some experiments [21]. A two parameter phenomenological model based on such behavior

$$\rho_{xx}(B) = \rho_{xx}(0)\left[1 - 2A + 2A/\sqrt{1+(\mu B)^2}\right]^{-1} \quad (1)$$

fits well at most gate voltages [19]. Here, $0 \leq A \leq 0.5$ is the quadratic coefficient of magnetoreresistance i.e. $\rho_{xx} = \rho_{xx,0}[1 + A(\mu B)^2 + \cdots]$ and μ is the carrier mobility. Fig. 3 shows the coherence peaks after subtracting the background from this classical contribution. In all figures, the plotted magnetoconductance is symmetrized with respect to field [19].

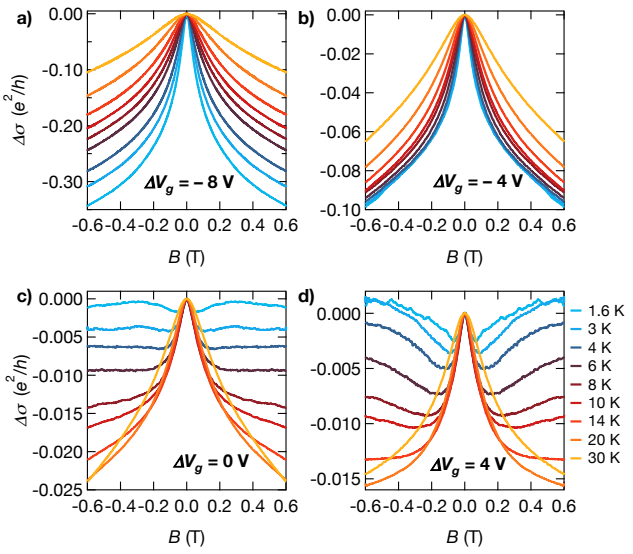

FIG. 2. Magnetoconductance, indicating weak antilocalization. (a-d) Differential longitudinal conductivity, $\Delta\sigma_{xx}(T,H) \equiv \sigma_{xx}(T,H) - \sigma_{xx}(T,0)$ versus magnetic field at temperatures between 1.6 K and 30 K at $V_g - V_{\rm min} = -8$ V (a), -4 V (b), 0 V (c), and 4 V (d)

Before proceeding, we provide quantitative estimates of the material parameters. From zero field transport and Hall coefficient ($R_{\rm H}$) data, we extract the density of charged impurities $n_{\rm imp} = (4.8 \pm 2.8) \times 10^{11}{\rm cm}^{-2}$ lying an average distance $d = 4.7$ nm from the 2DES plane, the dimensionless interaction parameter $r_s = 1.3 \pm 0.8$, and the characteristic charge density fluctuations $n_{\rm rms} = (1.2 \pm 0.2) \times 10^{11}{\rm cm}^{-2}$ [19].

DISCUSSION

Arrhenius activation of the conductivity at $V_g = V_{\rm min}$ confirms the presence of a surface gap. Gaps of order 100 meV have been observed through angle-resolved photoemission spectroscopy (ARPES) in 3D TI films thinner than 5 QLs [23, 24]. Our measured Arrhenius activation scale of 84 μeV is surprisingly small in comparison, even considering that our 8 QL film is thicker, and that Δ should decrease exponentially in film thickness. To explain the small value of $\Delta_{\rm Arr}$, we note that the clean-limit surface gap 2Δ could be smeared by disorder so that $\Delta_{\rm Arr} \ll \Delta$ [25]. Disorder smearing may also explain why many prior experiments on thin film 3D TIs do not observe a gap and instead see $\sigma > e^2/h$ at the CNP [26, 27].

At $\Delta V_g \lesssim -10$ V, we observed positive logarithmic temperature corrections to the conductivity. From the magnetoconductance, we know that WAL is present. WAL should contribute a negative temperature correction to conductivity:

$$\Delta\sigma_{xx}(T) = \frac{e^2}{\pi h}\alpha \log(T/T_0) \quad (2)$$

with $\alpha = -0.5$ per channel. Our observation of positive logarithmic corrections to conductivity with increasing temperature would naively indicate weak localization (WL), with $\alpha = 1$ rather than $= -0.5$. This apparent mismatch between the signs of the temperature and magnetoconductance corrections has been previously observed and resolved by including an electron-electron interaction (EEI) contribution to the conductivity [28–30]

$$\Delta\sigma_{\rm EEI}(T) = \frac{e^2}{2\pi h}\left(2 - \frac{3}{2}\tilde{F}_\sigma\right)\log(T/T_0)\,, \quad (3)$$

with screening factor $\tilde{F}_\sigma > 0$ [4]. The observation of overall positive temperature corrections to the conductivity means that the EEI correction dominates over the localization correction, in agreement with other experiments as well as calculations [31].

In principle, conventional 2DES cannot be metallic. Surprisingly, metallic temperature dependence (higher conductivity at lower temperature, even at milliKelvin temperatures) was found in semiconductor-based 2DES of exceptional cleanliness. This is now understood to result from EEI driving the system into a metallic phase. These systems transition to insulators as carrier density is reduced. Empirically, this transition consistently occurs when the conductivity is of order e^2/h in a variety of 2DES platforms including Si MOSFETs [32], GaAs/AlGaAs heterostructures [33, 34], graphene [35],

transition metal dichalcogenides [36], and even other 3D TI thin films [37].

In our system, electron-electron interactions have the opposite effect. As discussed above, EEI causes increasing conductivity with increasing temperature. We therefore never observe metallic temperature dependence in our device, despite the conductivity ranging from $6e^2/h$ at high carrier density to $< 0.01e^2/h$ ($T = 35$ mK) at $V_{\rm min}$ [19]. Nevertheless, unlike conventional 2DES, 3D TIs (in the limit $\Delta = 0$) are expected to have metallic single-particle descriptions. Is our system metallic? At the most fundamental level, a metal is characterized by delocalized electronic wavefunctions, not by the temperature dependance of its conductivity. Since here the temperature dependance of the resistivity fails to reflect even the presumed metallicity of the system at high doping, we must turn to the system's magnetoconductivity to address this question.

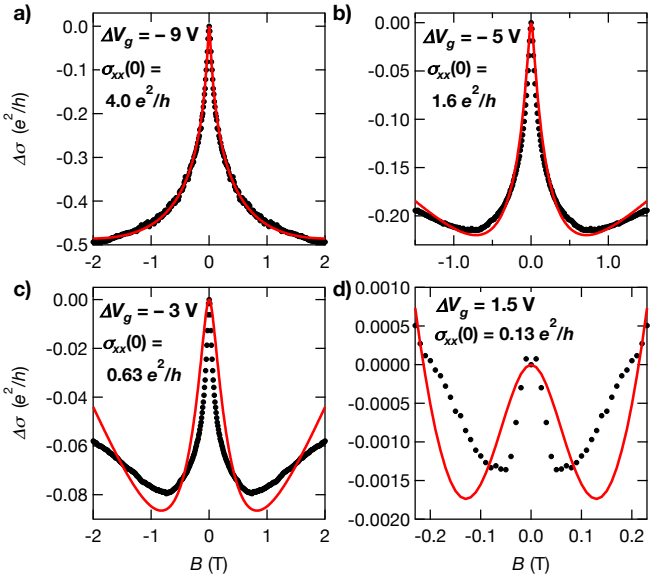

FIG. 3. Crossover of the quantum transport correction from weak anti-localization to weak localization. (a-d) Differential longitudinal conductivity, $\Delta\sigma_{xx}(T,H) \equiv \sigma_{xx}(T,H) - \sigma_{xx}(T,0)$ versus magnetic field at 1.6 K (black dots) at $V_g - V_{\rm min} = -9$ V (a), -5 V (b), -3 V (c), and 1.5 V (d). The classical contribution to the magnetoconductance has been subtracted from the data [19]. The absolute conductivity at $B = 0$ at each gate voltage is indicated. The HLN formula for WAL with a crossover to WL is fit to the data (red lines); the quality of fit becomes poor when $\sigma_{xx} \lesssim e^2/h$

In a 3D TI for which hybridization between the top and bottom surfaces is weak, electrons should exhibit weak antilocalization [38]. The magnetoconductance is given by the Hikami-Larkin-Nagaoka (HLN) formula [39]

$$\Delta\sigma = -\frac{e^2}{2\pi h} F\left(\frac{B}{B_\phi}\right), \tag{4}$$

where $F(x) = \ln(x) + \Psi(x + \frac{1}{2})$, Ψ is the digamma function, and $B_\phi = \hbar/(4el_\phi^2)$ the characteristic field associated with the electron coherence length l_ϕ. WAL is caused by the π Berry phase of the 2D Dirac dispersion, which suppresses backscattering.

We observe conventional quantum transport corrections at substantial hole doping. The WAL peak broadens with increasing temperature (Fig. 2 (a)). In theory, the peak should broaden as $l_\phi \propto T^{-p}$ with $p = 0.5$ in diffusive two dimensional metals. As shown in Fig. 4, we find that $p = 0.39$ at $\Delta V_g = -8$ V.

However, quantum corrections near the Dirac point differ from those at finite doping. At gate voltages more positive than $\Delta V_g = -4$ V, the magnetoconductivity becomes non-monotonic, qualitatively departing from equation (4). To understand this, recall that TSS hybridization in thin films should generate a Dirac mass (Δ), and the Berry phase $\phi_{\rm b}$ should deviate from π as $\phi_{\rm b} = \pi\,(1 - \Delta/E_F)$. The Berry phase thus should induce a crossover from perfect WAL ($\phi_{\rm b} = \pi$) in the massless (relativistic) limit to perfect WL ($\phi_{\rm b} = 0$) in the large mass (non-relativistic) regime [17, 40], with an associated magnetic field dependence of conductivity described by a modified HLN formula [41]

$$\Delta\sigma = -\frac{1}{2\pi}\frac{e^2}{h}\left[F\left(\frac{B}{B_\phi}\right) - 2F\left(\frac{B}{B_\phi + B_\Delta}\right) - F\left(\frac{B}{B_\phi + 2B_\Delta}\right)\right], \tag{5}$$

where $B_{\phi,\Delta} = \hbar/(4el_{\phi,\Delta}^2)$ are the characteristic fields associated with the coherence length l_ϕ and the crossover length scale l_Δ, respectively.

The quality of fits (Fig. 3) of equation (5) is greatly improved from that of equation (4), in exchange for an additional fitting parameter. We extract $l_\Delta \sim 40$ nm at all gate voltages. Unexpectedly, at the lowest field scales, we observe a WAL peak at *all* gate voltages, indicating that the system does not scale to strong localization, even when $\sigma \ll e^2/h$. Furthermore, the temperature dependence of the magnetoconductance peak at $V_g \approx V_{\rm min}$ is unusual, the WAL peak being more pronounced at *higher* temperatures (Fig. 2).

We note that the quality of fit becomes poor near $\Delta V_g = 0$, as shown in Fig. 3 (d). Here, the data have quantum corrections only at very small magnetic fields. We cannot make definitive statements about this observation since the quantum corrections are cleanly separable from the classical contribution to magnetoconductivity only for $\sigma \gg e^2/h$; thus, the HLN equation becomes invalid when $\sigma < e^2/h$. However, if the data at the smallest fields are interpreted as due to quantum corrections, the extracted l_ϕ still decays with increasing temperature according to a power law, albeit with power roughly half that expected from EEI. At present, we lack an explanation for this discrepancy.

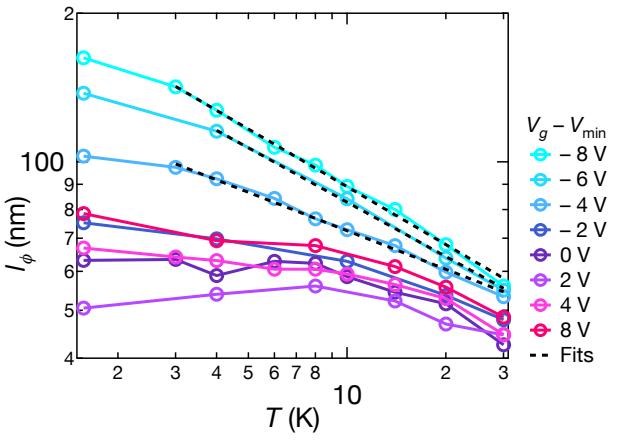

FIG. 4. Coherence lengths near the Dirac point. The characteristic coherence length l_ϕ, extracted from fitting equation (4) to the magnetoconductance, shown versus temperature at various gate voltages. A small range in B is chosen when fitting to isolate the lowest order contribution. l_ϕ is fit by a power law in temperature $l_\phi \propto T^{-p}$, yielding $p = 0.39$, 0.37, and 0.26 at $V_g - V_{\rm min} = -8$ V, -6 V, and -4 V, respectively. As V_g approaches $V_{\rm min}$, the temperature dependence of l_ϕ flattens at low temperature

We may use the extracted crossover length scale to estimate the clean-limit surface gap by dimensional analysis as $\Delta \approx \hbar v_F / l_\Delta = 6.7$ meV. This value is consistent with extrapolation from ARPES measurements of gaps for thinner films; as noted above, our measured transport gap $\Delta_{\rm Arr}$ is much smaller, presumably because we are not in the clean limit.

An interesting pattern in the literature is that WAL is observed in topological insulators having $\sigma_{xx} > e^2/h$, while WL is observed when $\sigma_{xx} \lesssim e^2/h$ [42]. This observation is explained by noting that WL in a topological insulator requires a mass gap around the Dirac point; since a gapped system insulates, we expect $\sigma_{xx} < e^2/h$. Our results contradict this pattern: at the smallest magnetic field scales (and therefore longest length scales), we observe a quantum coherence peak with negative magnetic field corrections at all carrier densities. This signature of WAL implies delocalized electronic states. Yet, this observation holds even at low carrier densities where the longitudinal conductivity falls well below e^2/h. Traditionally, $\sigma_{xx} \sim e^2/h$ is associated with reaching the Ioffe-Regel criterion $k_F l \approx 1$, which predicts that metallic 2DES do not exist at lower conductivities. Our results suggest that this device does not scale to strong localization, and instead enters an Ioffe-Regel-violating regime: a consequence of the symplectic character of the system together with disorder scattering. In the supplement, we theoretically justify this conclusion by finding self-consistent solutions in violation of the Ioffe-Regel limit for a low-energy model of massless 2D Dirac fermions for a broader range of the dimensionless parameters r_s and $n_{\rm imp} d^2$, using a combination of analytic and numeric results.

The authors thank Eli J. Fox, Hassan Shapourian, and Chi-Te Liang for insightful conversations, and Hava R. Schwartz for developments in our fabrication techniques. We are grateful for the contributions to instrumentation and measurement software by Andrew J. Bestwick, Eli J. Fox, Aaron L. Sharpe, and Menyoung Lee. Device fabrication and measurement was supported by the U.S. Department of Energy, Office of Science, Basic Energy Sciences, Materials Sciences and Engineering Division, under Contract DE-AC02-76SF00515. Infrastructure and cryostat support were funded in part by the Gordon and Betty Moore Foundation through Grant No. GBMF3429. Part of this work was performed at the Stanford Nano Shared Facilities (SNSF), supported by the National Science Foundation under award ECCS-1542152. The theoretical work in Singapore was funded by the National University of Singapore Young Investigator Award (R-607-000-094-133), and the Singapore Ministry of Education (MOE2017-T2-1-130). The work at Rutgers was supported by the Gordon and Betty Moore Foundation's EPiQS Initiative (GBMF4418) and the National Science Foundation (NSF) (EFMA-1542798).

* E-mail: goldhaber-gordon@stanford.edu

[1] L. Fu, C. L. Kane, and E. J. Mele, Physical Review Letters **98**, 106803 (2007).
[2] H. Zhang, C.-x. Liu, X.-l. Qi, X. Dai, Z. Fang, and S.-c. Zhang, Nature Physics **5**, 438 (2009).
[3] Y. Xia, D. Qian, D. Hsieh, L. Wray, A. Pal, H. Lin, A. Bansil, D. Grauer, Y. S. Hor, R. J. Cava, and M. Z. Hasan, Nature Physics **5**, 398 (2009).
[4] P. A. Lee and T. V. Ramakrishnan, Reviews of Modern Physics **57**, 287 (1985).
[5] K. Nomura, M. Koshino, and S. Ryu, Physical Review Letters **99**, 146806 (2007).
[6] J.-H. Chen, W. G. Cullen, C. Jang, M. S. Fuhrer, and E. D. Williams, Physical Review Letters **102**, 236805 (2009).
[7] J. Linder, T. Yokoyama, and A. Sudbø, Physical Review B **80**, 205401 (2009).
[8] H. Z. Lu, W. Y. Shan, W. Yao, Q. Niu, and S. Q. Shen, Physical Review B **81**, 115407 (2010).
[9] J. Chen, H. J. Qin, F. Yang, J. Liu, T. Guan, F. M. Qu, G. H. Zhang, J. R. Shi, X. C. Xie, C. L. Yang, K. H. Wu, Y. Q. Li, and L. Lu, Physical Review Letters **105**, 176602 (2010).
[10] J. Zhang, C.-Z. Chang, Z. Zhang, J. Wen, X. Feng, K. Li, M. Liu, K. He, L. Wang, X. Chen, Q.-K. Xue, X. Ma, and Y. Wang, Nature Communications **2**, 574 (2011).
[11] N. Koirala, M. Brahlek, M. Salehi, L. Wu, J. Dai, J. Waugh, T. Nummy, M.-G. Han, J. Moon, Y. Zhu, D. Dessau, W. Wu, N. P. Armitage, and S. Oh, Nano Letters **15**, 8245 (2015).
[12] B. Skinner, T. Chen, and B. I. Shklovskii, Journal of Experimental and Theoretical Physics **117**, 579 (2013).

[13] N. Borgwardt, J. Lux, I. Vergara, Z. Wang, A. A. Taskin, K. Segawa, P. H. Van Loosdrecht, Y. Ando, A. Rosch, and M. Grüninger, Physical Review B **93**, 245149 (2016).

[14] D. Nandi, B. Skinner, G. H. Lee, K.-F. Huang, K. Shain, C.-Z. Chang, Y. Ou, S.-P. Lee, J. Ward, J. S. Moodera, P. Kim, B. I. Halperin, and A. Yacoby, Physical Review B **98**, 214203 (2018).

[15] Y. S. Kim, M. Brahlek, N. Bansal, E. Edrey, G. A. Kapilevich, K. Iida, M. Tanimura, Y. Horibe, S. W. Cheong, and S. Oh, Physical Review B - Condensed Matter and Materials Physics **84**, 073109 (2011).

[16] Y. Jiang, Y. Wang, M. Chen, Z. Li, C. Song, K. He, L. Wang, X. Chen, X. Ma, and Q. K. Xue, Physical Review Letters **108**, 016401 (2012).

[17] M. Lang, L. He, X. Kou, P. Upadhyaya, Y. Fan, H. Chu, Y. Jiang, J. H. Bardarson, W. Jiang, E. S. Choi, Y. Wang, N. C. Yeh, J. Moore, and K. L. Wang, Nano Letters **13**, 48 (2013).

[18] M. Salehi, H. Shapourian, I. Rosen, M.-G. Han, J. Moon, P. Shibayev, D. Jain, D. Goldhaber-Gordon, and S. Oh, arXiv:1903.00489 (2019).

[19] See the supplemental materials for more information..

[20] N. Ramakrishnan, Y. T. Lai, S. Lara, M. M. Parish, and S. Adam, Physical Review B **96**, 224203 (2017).

[21] S. Cho and M. S. Fuhrer, Physical Review B **77**, 081402 (2008).

[22] J. Ping, I. Yudhistira, N. Ramakrishnan, S. Cho, S. Adam, and M. S. Fuhrer, Physical Review Letters **113**, 047206 (2014).

[23] Y. Zhang, K. He, C.-Z. Chang, C.-L. Song, L.-L. Wang, X. Chen, J.-F. Jia, Z. Fang, X. Dai, W.-Y. Shan, S.-Q. Shen, Q. Niu, X.-L. Qi, S.-C. Zhang, X.-C. Ma, and Q.-K. Xue, Nature Physics **6**, 584 (2010).

[24] M. Neupane, A. Richardella, J. Sánchez-Barriga, S. Xu, N. Alidoust, I. Belopolski, C. Liu, G. Bian, D. Zhang, D. Marchenko, A. Varykhalov, O. Rader, M. Leandersson, T. Balasubramanian, T.-R. Chang, H.-T. Jeng, S. Basak, H. Lin, A. Bansil, N. Samarth, and M. Z. Hasan, Nature Communications **5**, 3841 (2014).

[25] C. Z. Chang, W. Zhao, J. Li, J. K. Jain, C. Liu, J. S. Moodera, and M. H. Chan, Physical Review Letters **117**, 126802 (2016).

[26] Y. Zhang, T.-T. Tang, C. Girit, Z. Hao, M. C. Martin, A. Zettl, M. F. Crommie, Y. R. Shen, and F. Wang, Nature **459**, 820 (2009).

[27] T. Taychatanapat and P. Jarillo-Herrero, Physical Review Letters **105**, 166601 (2010).

[28] J. Wang, A. M. DaSilva, C.-Z. Chang, K. He, J. K. Jain, N. Samarth, X.-C. Ma, Q.-K. Xue, and M. H. W. Chan, Physical Review B **83**, 245438 (2011).

[29] H.-Z. Lu and S.-Q. Shen, Proc.SPIE **9167**, 91672E (2014).

[30] H. Choi, S. Jung, T. H. Kim, J. Chae, H. Park, K. Jeong, J. Park, and M.-H. Cho, Nanoscale **8**, 19025 (2016).

[31] H.-Z. Lu and S.-Q. Shen, Physical Review Letters **112**, 146601 (2014).

[32] S. V. Kravchenko, W. E. Mason, G. E. Bowker, J. E. Furneaux, V. M. Pudalov, and M. DIorio, Physical Review B **51**, 7038 (1995).

[33] Y. Hanein, U. Meirav, D. Shahar, C. C. Li, D. C. Tsui, and H. Shtrikman, Physical Review Letters **80**, 1288 (1998).

[34] M. Y. Simmons, A. R. Hamilton, M. Pepper, E. H. Linfield, P. D. Rose, D. A. Ritchie, A. K. Savchenko, and T. G. Griffiths, Physical Review Letters **80**, 1292 (1998).

[35] F. Amet, J. R. Williams, K. Watanabe, T. Taniguchi, and D. Goldhaber-Gordon, Physical Review Letters **110**, 216601 (2013).

[36] B. Radisavljevic and A. Kis, Nature Materials **12**, 815 (2013).

[37] J. Liao, Y. Ou, X. Feng, S. Yang, C. Lin, W. Yang, K. Wu, K. He, X. Ma, Q.-K. Xue, and Y. Li, Physical Review Letters **114**, 216601 (2015).

[38] P. Adroguer, W. E. Liu, D. Culcer, and E. M. Hankiewicz, Physical Review B **92**, 241402 (2015).

[39] S. Hikami, A. I. Larkin, and Y. Nagaoka, Progress of Theoretical Physics **63**, 707 (1980).

[40] L. Zhang M. Dolev, Q. I. Yang, R. H. Hammond, B. Zhou, A. Palevski, Y. Chen, and A. Kapitulnik, Physical Review B **88**, 121103 (2013).

[41] S. V. Iordanskii, Y. B. Lyandageller, and G. E. Pikus, JETP Letters **60**, 206 (1994).

[42] Q. I. Yang and A. Kapitulnik, Physical Review B **98**, 081403 (2018).